PROFILES FOR REVERSIBLE AXIAL FANS

Georg KLEPP, Markus FILIPPI

IFE, Hochschule Ostwestfalen-Lippe,

Liebigstraße 87 32657 Lemgo, Germany

SUMMARY

In order to achieve full reversibility for axial flow fans, blades with double-cambered or S-cambered profiles may be used. In a numerical analysis the performance of S-cambered profiles is investigated. The flow field is computed with the RANS equations and the resulting lift and drag forces are derived. The influence of camber and thickness is investigated. Possibilities for optimizing fully reversible profiles are highlighted.

INTRODUCTION

Most fans have a distinct flow direction, nevertheless a reversible flow direction for fans is desirable in certain circumstances in ventilation and drying applications. For fully reversible axial fans flow characteristics and performance are independent of the flow direction. The flow direction is changed by reversing the rotational direction. In order for the fan performance to be similar in both directions, the blade profiles of these fans have to be point symmetric. Most common are elliptical type profiles and twice cambered or S-shaped profiles.

Elliptical type profiles are elliptical, lense-shaped or thick plates with rounded edges. These profiles are point symmetric, nevertheless as also the upper and the lower side of the profile are symmetric as well, the aerodynamic performance is inferior to airfoils. For elliptical profiles lift and drag strongly depend on the Reynoldsnumber, in the range between $3 \cdot 10^5$ and $3 \cdot 10^6$. With decreasing thickness this dependency diminishes. At higher Reynoldsnumbers elliptical profiles have a lesser lift curve slope then standard airfoils due to the different length of attached flow on the upper and lower surfaces, [3]. The performance of lense shaped single profiles and cascades were computed in [4].

It is desirable to have the aerodynamic performance of airfoils but also the attribute of reverseability. One possible approach is to use S-shaped or double cambered profiles, i.e. to shape airfoils to a point symmetric geometry. For fully reversible axial flow machines these are more efficient than conventional single cambered profiles, [1]. These shapes are mostly derived from existing profiles using a twice cambered (i.e. S-shaped) camber-line. The maximum thickness is at the middle of the profile. The thickness distribution and the function of the camberline can then be arbitrarily chosen.

One such class of profiles are based on the NACA 0010-35 thickness distribution (up to the maximum thickness) and a parabolic function for the camberline.

One of these profiles based on NACA 0010-35, the profile S3525 (S cambered, 3% thickness, 5% camber, maximum camber at 25%) was extensively investigated experimentally for Re=4.5 10^5 as it is used in tidal turbines, [1]. The flow is influenced by the pressure gradient as well as the curvature, which changes along the profile length. At the ends of the profile the pressure gradient on the upper surface is negative and on the lower surface positive. Between the maximum camber and the minimum camber the pressure gradient on the upper side is negative and on the lower side positive. Before the middle of the profile is reached, a separation bubble is found on the upper surface around the point of maximum thickness. On the lower surface of the profile the flow separates at the leading edge and reattaches shortly after the point of maximum camber.

In [2] a k-kl-omega three equation transitional turbulence model is recommended for the computation of the flow around S-cambered profiles at lower Reynolds numbers (Re=4.5 10^5) in order to correctly assess the transition from laminar to turbulent flow.

Apart from these specific investigations, data for various types of S-cambered profiles is scarce. In order to assess the potential of these profiles for fan applications the flow around such S-shaped reversible profiles is investigated and compared to the flow over elliptical profiles. Thus it is possible to get further insight into the aerodynamics in order to improve the efficiency of the profile design for fully reversible axial fans.

APPROACH

In order to facilitate this approach a new type of S-profile is defined. The basic thickness distribution is elliptic, described by the diameter ratio. The maximum thickness is thus at the middle of the profile.

The camber line is described by the sine-function with the amplitude coinciding with the maximum camber and the total length of unity. The maximum camber is therefor located at ¼, the maximum thickness at ½ and the minimum camber at ¾. Thus the influence of the camber can be easily assessed by comparison to the flow around the corresponding elliptic profile.
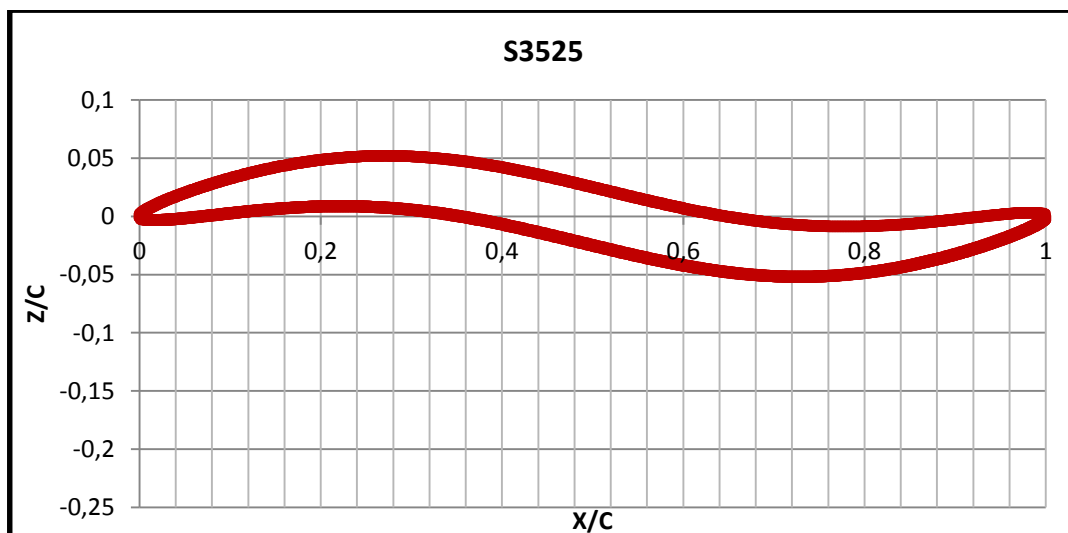
Figure 1: S-shaped profile S-3-5-25

A comparison with an S3525 (S-3-5-25: 3% camber at 25% profile length and 5% maximum thickness) as defined in [1], [2] shows only slight deviations in the geometry.

An experimental investigation would be expensive, therefore the assessment and comparison of the influence of different parameters using a numerical model seems more convenient. As the flow pattern is strongly influenced by flow separation and reattachment due to interaction in the boundary layer, a modelling approach based on the Reynolds-averaged Navier-Stokes (RANS) seems appropriate.

In order to get an insight into the flow patterns evolving, the flow over the profiles is investigated numerically solving the two dimensional incompressible Reynolds averaged Navier-Stokes (RANS) equations. The flow around various profiles at various incident angles and for Reynoldsnumbers, as appropriate for fan profile applications, is computed. As we focus on higher Reynoldsnumbers, we will neglect transitional effects and use standard turbulence models for the flow around profiles,

The flow patterns of the flow around the profiles are investigated and the lift coefficient and drag coefficient are derived from the computations.

NUMERICAL SET UP

The length and the height of the twodimensional computational flow domain is sixteen times larger than the length of the profile. The solution is computed on a blockstructured O-shaped hexaedral grid. The grid is staggered and refined near the wall in order to achieve yplus values smaller then one. The grid independence is established.

An inflow boundary condition with a prescribed velocity vector is defined on the boundary in front of the profile, an outflow condition is prescribed for the rest of the boundary.

The Navier-Stokes equations are discretized with a second order accurate finite volume scheme. The turbulence is modeled using the Spalart-Allmaras model without wall functions. Most of the computations were stationary, the pressure coupling is achieved by the SIMPLE algorithm.

The simulations are performed with openFoam 4.0. The models mentioned above (turbulence models, pressure coupling) are all used as implemented in openFoam [5].

In addition the polar diagram around an S-shaped profile is computed based on the panel-method [5] in order to assess the deviations.

VALIDATION

In order to validate the numerical method, we restrict ourselves to the S-shaped profile, as the flow around S-shaped profiles is more challenging then the flow around elliptical profiles.

For the profile S3525 measured data (incident angle 0°, Reynoldsnumber 4.5 10^5) is available [1]. The computations were performed with the panel-method [6] and stationary with the Spalart-Allmaras model.

The values computed with the panel method deviate significantly from the measured data as the important viscous effects in the boundary layer influencing the flow pattern are not appropriately taken into account. Thus as expected these methods should be omitted in predicting the performance of S-shaped profiles.

The computations with the stationary RANS equations are more successful. After 60,000 -130,000 iteration steps the residuals are smaller then 10^{-5} and the lift and drag coefficients converge to constant values although there is some scatter (smaller 0,1%) in the values. This might be due to numerical errors as well as transient effects that are neglected in the stationary computation.
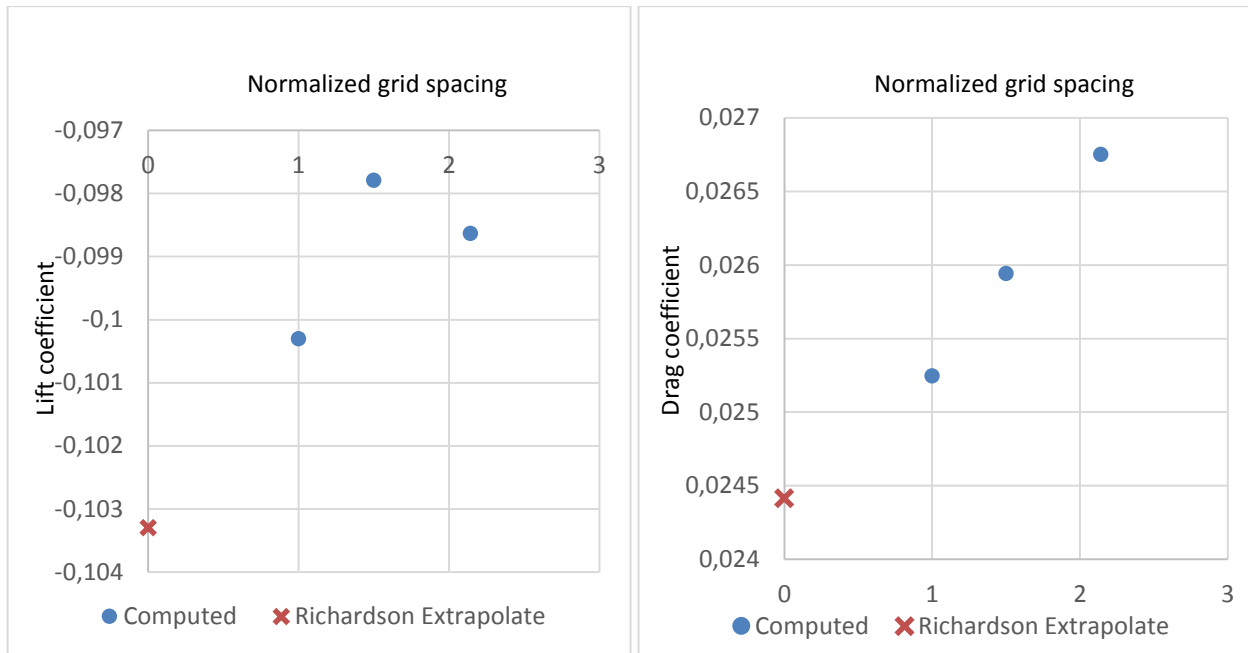
Figure 2: Grid convergence study: lift and drag coefficients vs. normalized grid spacing

For the profile S-15-5-25 (Reynoldsnumber $4.5 \cdot 10^5$) a grid convergence study was performed according to the procedure outlined in [7]. For the coarse grid (117,600 cells) the asymptotic range was not reached. Acceptable results are computed with the intermediate grid (240,00 cells) and the fine grid (540,000 cells). The y^+ values in the computations are all smaller than 1. For the analysis the computations are performed using the intermediate grid.
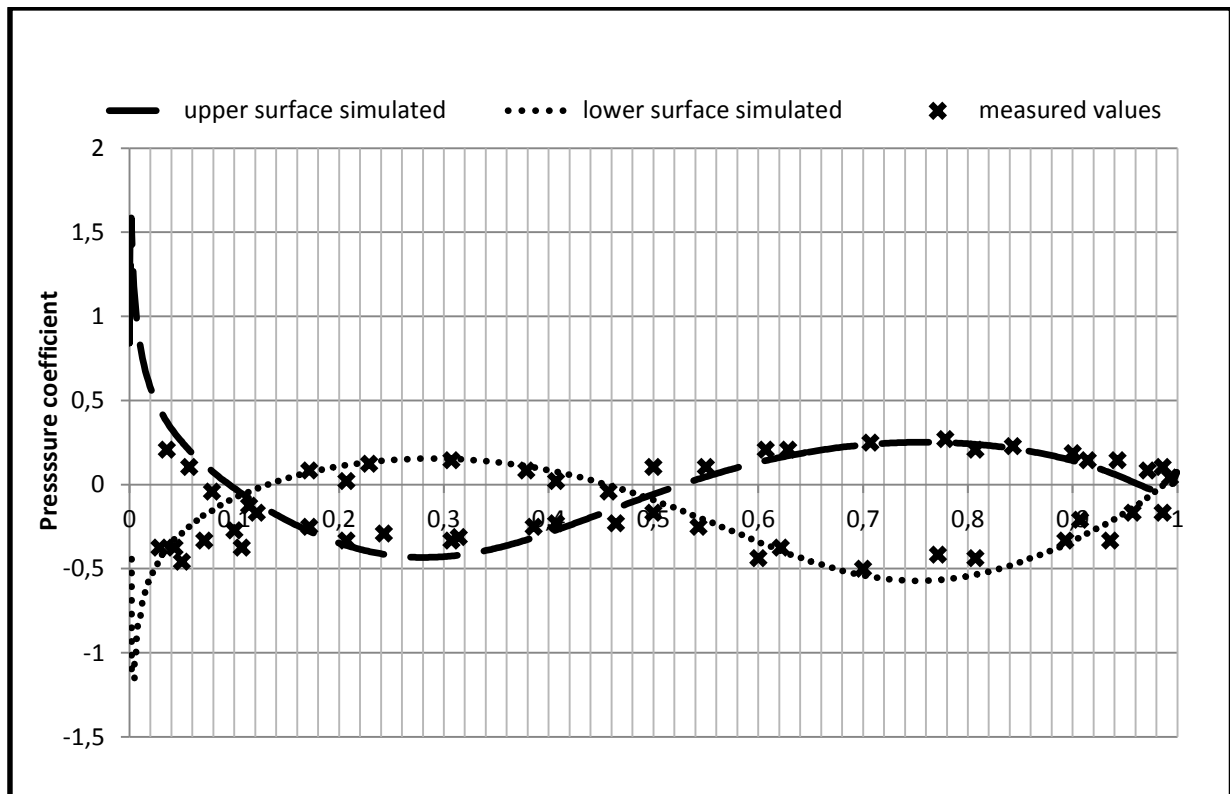
Figure 3: Distribution of pressure coefficient on upper and lower surface, measured [1] and computed values S3525.

For the profile S3525 the measured [1] and computed pressure distribution (Reynoldsnumber 4.5 10^5) and thus the resulting lift and drag coefficients are in adequate agreement: lift coefficient -0.181 computed and -0.207 measured, drag coefficient 0.037 computed and 0.018 measured. Deviations (order of magnitude 0.02) are due to the measurement errors, the influence of surface roughness and turbulence intensity on the separation and reattachment, the neglect of transitional flow at the tip of the profile, the neglect of transient effects and the limitations of the turbulence model.

For this comparative numerical analysis, the stationary approach with the Spalart-Allmaras turbulence model is feasible for computing the flow around the elliptical and S-shaped profiles.

RESULTS

The flow around various profiles (thickness 3% to 17%) at various incident angles (-2° to 15°) and for various Reynolds numbers (4.5 10^5 and 2.575 10^6), is computed. The flow patterns of the flow around the profiles are investigated and polar diagrams are derived from the computations.

Flow pattern

The flow around the S-cambered profiles may be divided in three regions: leading edge up to maximum camber, maximum camber up to minimum camber and minimum camber up to trailing edge.

In the first region the flow is similar to the flow around an elliptical profile at a higher incidence angle. The additional incidence is caused by the curvature of the camber-line.

Depending on the course of the profile surface, determined by camber and thickness, the flow mostly separates in the second region.

Caused by the camber, in the first region the pressure at the leading edge is negative on the lower side and positive on the upper side. The pressure on the upper side has a negative gradient until it reaches its minimum near the point of maximum camber. The pressure on the lower side has a positive gradient until it reaches its maximum near the point of maximum camber. After the maximum (in the middle of the profile) the pressure on the upper surface is positive and on the lower surface is negative. Thus only the first half of the profile, apart from the effects at the leading edge has a significant contribution to the lift coefficient. The influence of the trailing

half of the profile is neglectable. The main contribution to the drag coefficients comes from the pressure peak at the leading edge on the upper side.
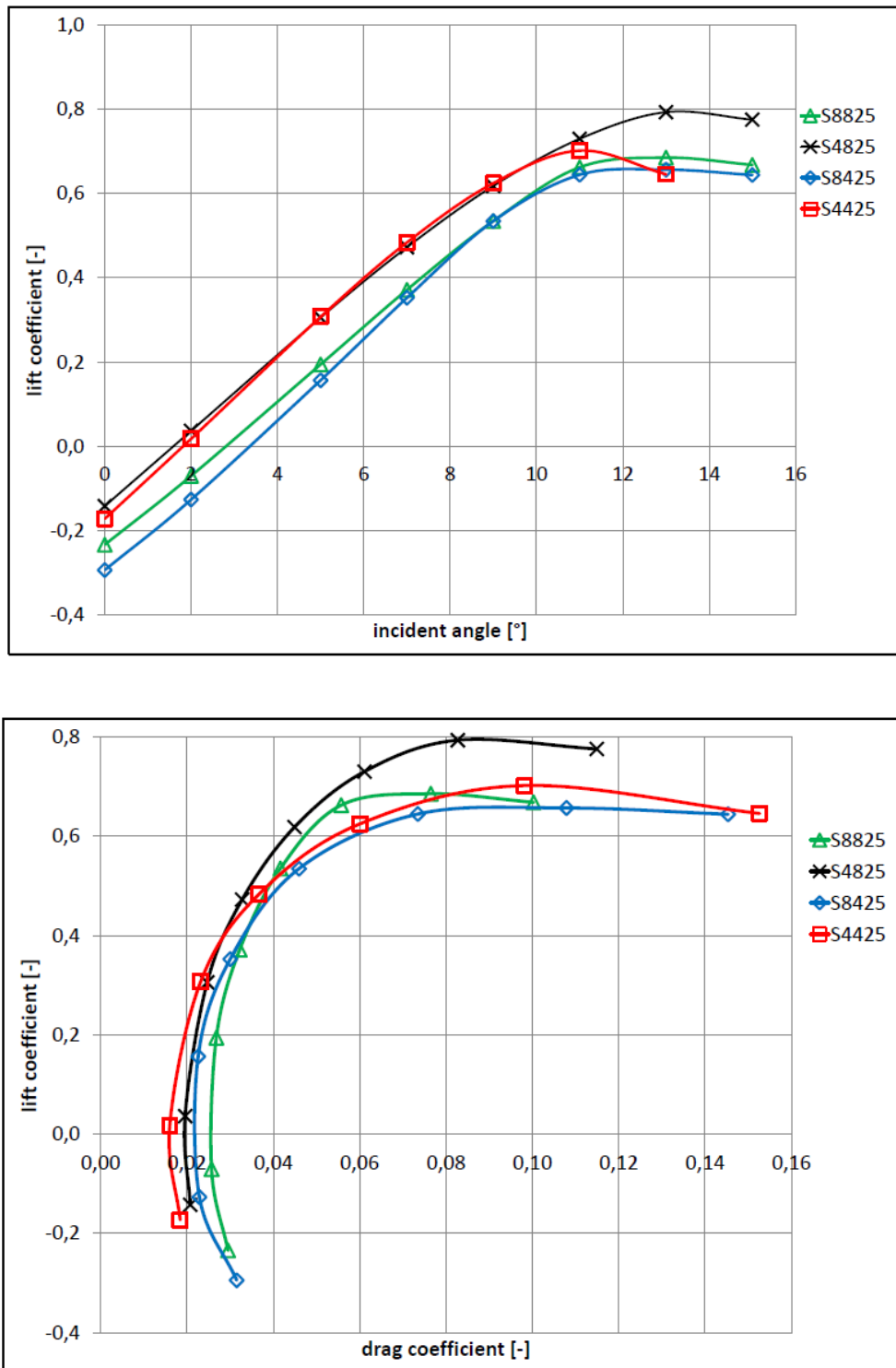
Figure 4: Polar diagrams S8825, S4825, S8425, S4425 Re=25.75 10^6.

Lift, drag and incident angle

With an increase in camber and profile thickness lift and drag also increases. The most important parameter is the camber. The thickness distribution has a smaller influence. Due to the S-shape the flow is asymmetric and complex: There is always flow separation as well as reattachment and changes in the direction of the pressure gradient due to the curvature changes. For strongly cambered profiles, these effects leading to strong separation bubbles are predominant and the advantages using a twice cambered profile might diminish.

The camber of the S-profile has the predominant influence. The influence of the camber is more significant for thin profiles and less significant for profiles with higher thickness.

For a zero incident angle the S-shape leads to an increase in drag and the lift coefficient changes to negative values. With an increase in the incident angle the drag coefficient increases further and the lift coefficient increases (back to positive values). With increasing camber the lift coefficient first decreases (especially for thin profiles) and then increases again (especially for thick profiles). For bigger camber the drag is higher and the stall conditions occur at smaller incident angles.

With an increase in thickness the drag forces increase significantly. The lift forces increase slightly. The latter effect is enhanced by the camber of the profile.

Increasing the Reynoldsnumber leads to a slight increase in lift and a significant reduction in drag. These effects are more distinct for the strong cambered and thick profiles.

CONCLUSION

Based on this analysis it is possible to derive design recommendations for an improved design of reversible profiles. For the S-shaped profile only little camber is required to improve the performance compared with an elliptic profile. Increasing camber leads to a significant increase in drag. The geometry as defined here for S-cambered profiles can only be a starting point for an optimized profile geometry. An adjustment of the profile curvature independent of the shape defined by formulas seems sensible

For an investigation with quantitive resilient results specific care should be given to the turbulence model used. A transient simulation using an appropriate turbulence model (e.g. as proposed in [2]) seems appropriate to capture the complex flow features with adequate precision to compute quantitative reliable results.

.

REFERENCES

[1] R.S. Madhusudan et al : *Boundary layer studies over an S-blade*. Fluid Dynamics Research 14 241-258 Elsevier, **1994**

[2] M. Premkumar T, D. Chatrejee: *Computaional analysis of flow over a cascade of S-shaped hydrofoil of fully reversible pump-turbine used in extgracting tidal anergy*. Renewable Energy 7 (2015) 240 – 249 Elsevier **2015**

[3] R.A. Wallis - *Axial Flow Fans and Ducts*. New York: Wiley **1983**

[4] Z.T. Spasic et al – Low-pressure reversible axial fan with straight profile blades and relatively high efficiency. Thermal Science, vol. 16, 2, pp. S593-S60 Vinca **2012**

[5] openFoam 4.0 *Documentation* https://cfd.direct/openfoam/user-guide/

[6] JavaFoil *Documentation* https://www.mh-aerotools.de/airfoils/javafoil.htm

[7] P. J. Roache – *Quantification of uncertainty in computational fluid dynamics* Annu. Rev. Fluid. Mech. 29:123–60 **1997**

ANNEXES
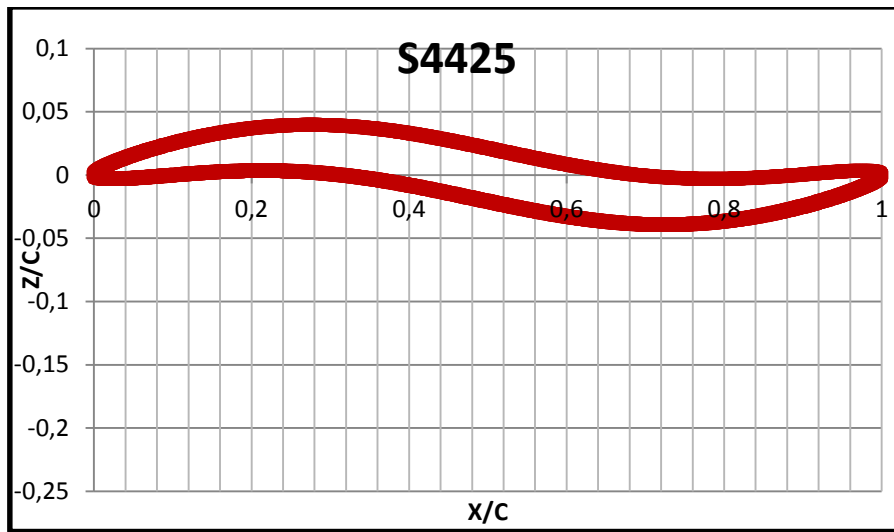
A1 Profile S4425
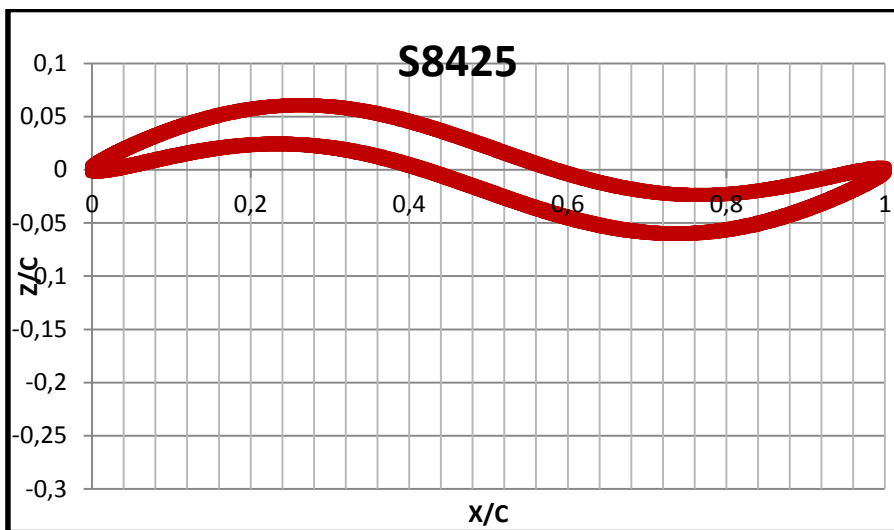
A2 Profile S8425
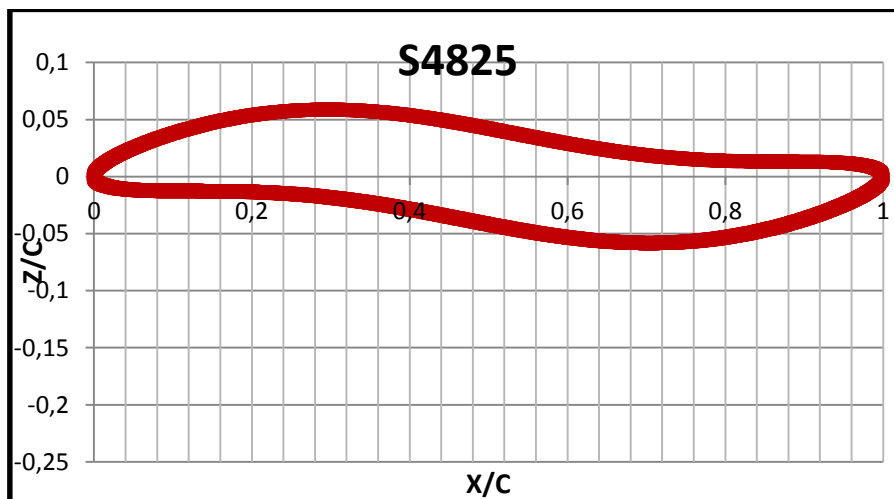
A3 Profile S4825
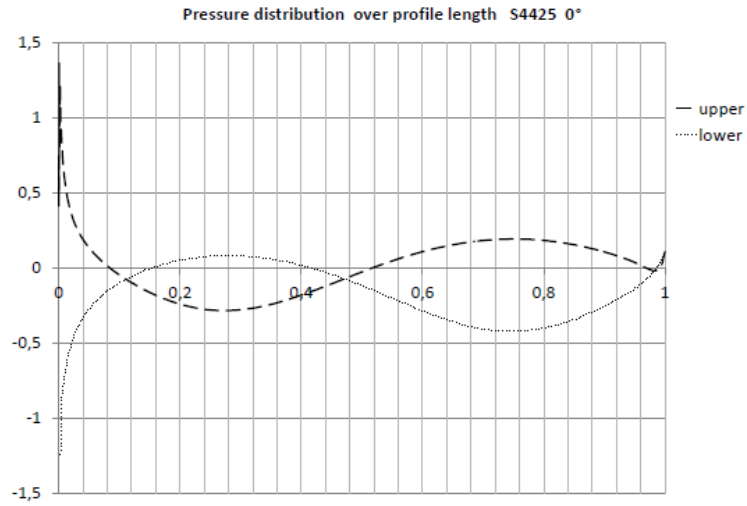
Pressure distribution over profile length   S4425 0°

A4 Distribution of pressure coefficient on upper and lower surface S4425 incident angle 0° Re=25.75 10^6

Pressure distribution over profile length   S4425 5°

A5 Distribution of pressure coefficient on upper and lower surface S4425 incident angle 5° Re=25.75 10^6

Pressure distribution over profile length   S4425 13°
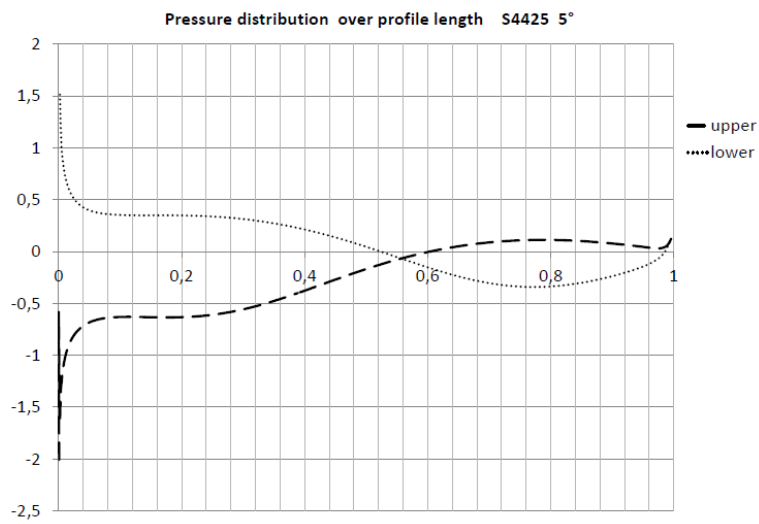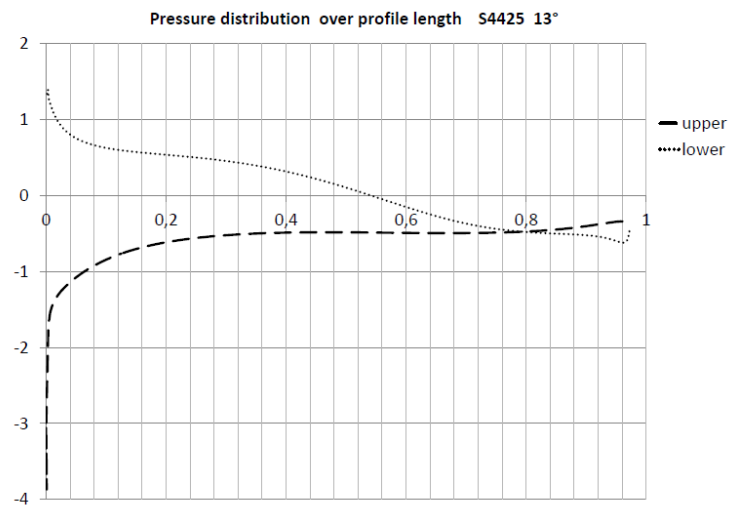
A6 Distribution of pressure coefficient on upper and lower surface S4425 incident angle 13° Re=25.75 10^6
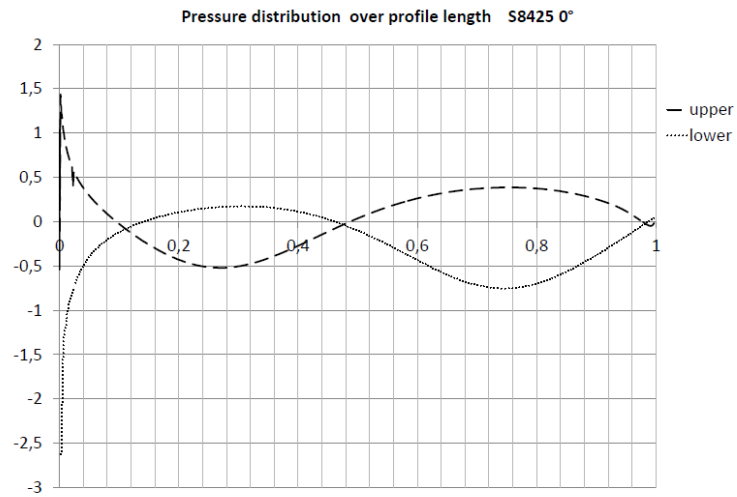
A7 Distribution of pressure coefficient on upper and lower surface S8425 incident angle 0° Re=25.75 10⁶
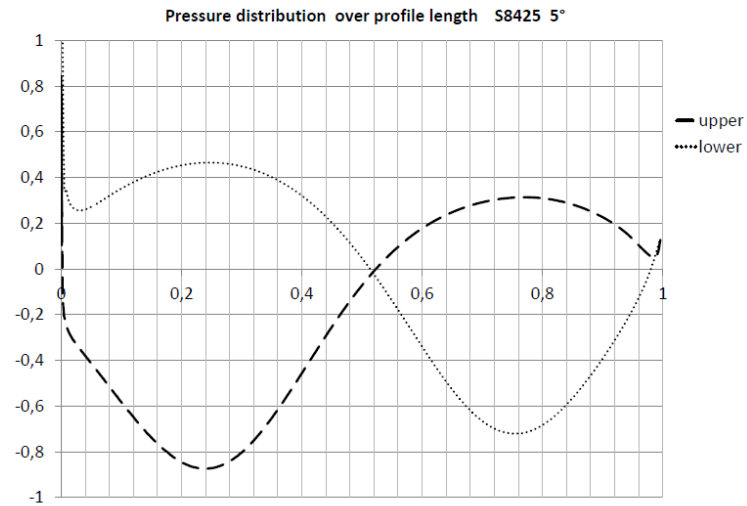
A8 Distribution of pressure coefficient on upper and lower surface S8425 incident angle 5° Re=25.75 10⁶
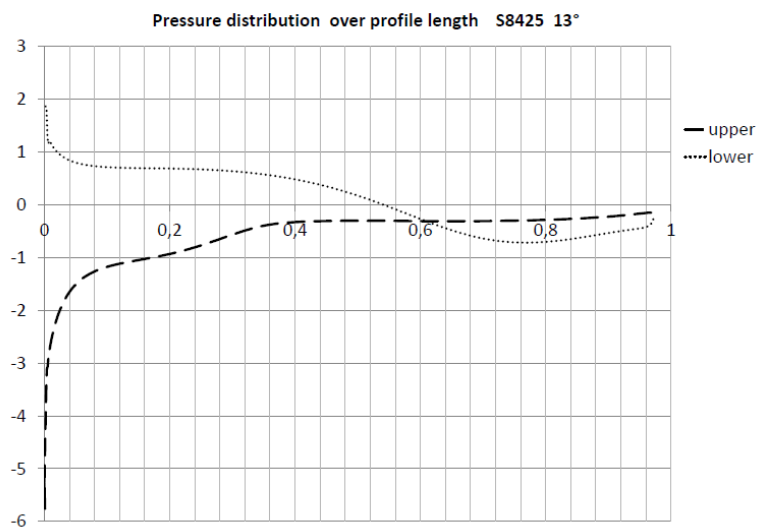
A9 Distribution of pressure coefficient on upper and lower surface S8425 incident angle 13° Re=25.75 10⁶
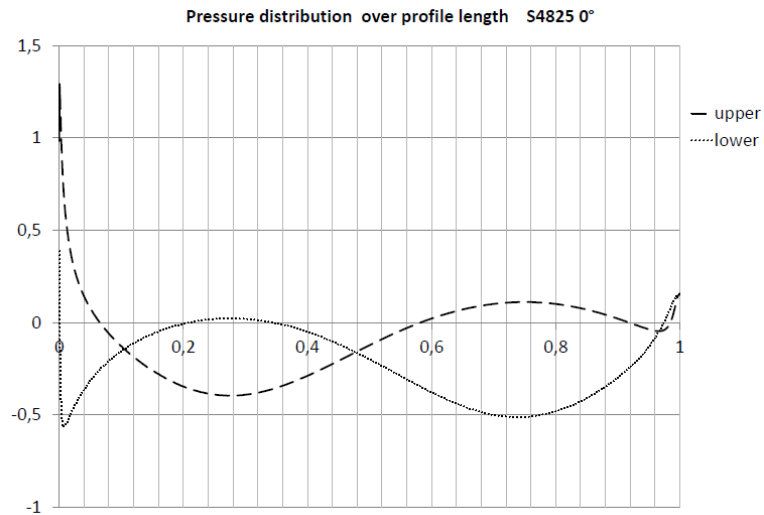
A10 Distribution of pressure coefficient on upper and lower surface S4825 incident angle 0° Re=25.75 10⁶
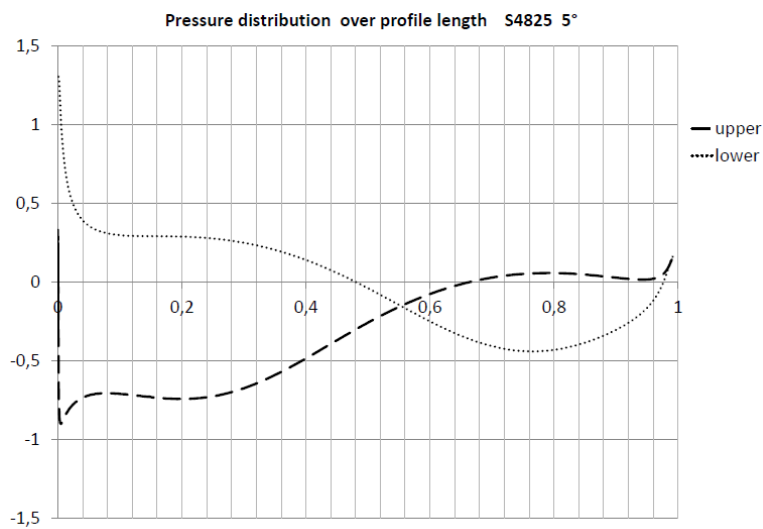
A11 Distribution of pressure coefficient on upper and lower surface S4825 incident angle 5° Re=25.75 10⁶

A12 Distribution of pressure coefficient on upper and lower surface S4825 incident angle 13° Re=25.75 10⁶